Title

ANALYSIS OF THE OPERATION OF POROUS GAS ELECTRODES WITH TWO SUPERIMPOSED SCALES OF PORE STRUCTURE

Author

Grens, Edward S.

Publication Date

1965-11-01

UCRL-16529

University of California

Ernest O. Lawrence Radiation Laboratory

ANALYSIS OF THE OPERATION OF POROUS GAS ELECTRODES WITH TWO SUPERIMPOSED SCALES OF PORE STRUCTURE

DISCLAIMER

UCRL-16529

UNIVERSITY OF CALIFORNIA

Lawrence Radiation Laboratory
Berkeley, California

AEC Contract No. W-7405-eng-48

ANALYSIS OF THE OPERATION OF POROUS GAS ELECTRODES WITH TWO SUPERIMPOSED SCALES OF PORE STRUCTURE

Edward A. Grens II

November 1965

ANALYSIS OF THE OPERATION OF POROUS GAS ELECTRODES WITH TWO SUPERIMPOSED SCALES OF PORE STRUCTURE

by

Edward A. Grens II
Inorganic Materials Research Division,
Lawrence Radiation Laboratory, and
Department of Chemical Engineering
University of California, Berkeley

ABSTRACT (BRIEF)

Many of the types of porous gas electrodes used in fuel cells have a double porosity structure: a system of gas filled macropores superimposed on one of liquid filled micropores. A model for the operation of such an electrode is formulated by considering the macro and micropore systems as parallel one dimensional continua, appropriately joined by a series of "linking pores" which represent the micropore structure immediately surrounding each macropore. Transport of dissolved gas reactant, ionic species, and current to/from reaction sites in the linking and micropores is analyzed, together with local electrode kinetic relationships, to characterize the reaction distribution and exterior behavior for the electrode. The calculated behavior for an oxygen cathode operating in 6.9 N KOH illustrates the high activity and almost linear overpotential/current relationship predicted by this model. There are significant differences in electrode behavior from that predicted by available treatments based on a single pore or uniform pore structure.

In the search for efficient porous gas electrodes for fuel cell systems, rather complex electrode structures are being utilized. The majority of these involve a multiple scale of porosity, that is, a pore size distribution characterized by major contributions to the electrode void fraction in two (or more) widely separated pore diameter ranges. This multiple porosity exists in the body of the electrode, quite apart from any layer of small pore diameter material provided for interface control[4,10], and is usually the result of forming the electrode from a fine powder which is in itself porous. Such a structure is found in carbon[7], black platinum[6], and Raney alloy electrodes[4]; it is well described, for carbon, by Paxton and coworkers[7].

In a double porosity scale electrode the pores can be subdivided into two systems: the larger or macropores (perhaps 1-50μ diameter) which are filled with reactant gas, and the smaller or micropores (perhaps 0.1μ or less diameter) which are flooded with electrolyte by capillarity. The macro and micropores exist as superimposed systems throughout the entire electrode, the micropores intersecting the walls of the macropores, as illustrated in highly idealized form in Figure 1. The reactant gas enters the macropores at the gas side of the electrode and dissolves in the electrolyte at the "mouths" of the micropores along the walls of the larger pores. From there the gas diffuses in solution to reaction sites along the walls of the micropores. The ionic species in the electrolyte that participate in the reaction (and carry the current) diffuse and migrate through the micropore system between the reaction site and the bulk electrolyte at the liquid side of the electrode. Electronic current to reaction sites is carried by the conducting matrix of the electrode.

Gas electrodes for which the pores are all much the same size, and in

which the reaction occurs under an electrolyte film on the walls of largely gas filled pores, have been quite extensively analyzed[8,9,2,3]. Reaction in the liquid filled parts of such pores with gas supply by surface diffusion has also been considered[4,3]. Electrodes in which all pores are flooded have been treated, but these are not efficient and of relatively little interest. No uniform porosity model seems capable of explaining the performance of some of the more active electrodes (e.g. [6]) without adopting unreasonable values for one or more system parameters. However, the electrode with a double scale of porosity has received very little theoretical consideration. It has been subjected to a much simplified preliminary analysis by Burshstein and coworkers, primarily for the purpose of investigating the effects of changing, by pressure adjustments, the fraction of pores which are gas filled[1]. In that treatment transport of dissolved gas and ionic species was not considered, and a linear kinetic expression without concentration effect was utilized.

In the present investigation the gas electrode with superimposed systems of macropores containing a pure reactant gas and micropores filled with electrolyte was analyzed at the steady state. Transport of dissolved gas and of ionic species were taken into consideration, and, in fact, are the processes largely determining electrode performance. A realistic electrode kinetic expression including concentration effects and forward and reverse reaction terms was used.

MODEL FOR THE GAS ELECTRODE WITH DOUBLE SCALE OF POROSITY

The actual porous electrode consists of a very complex arrangement of interconnected voids, or pores, in a condusting solid matrix. However, so long as the characteristic dimensions of both the macro and micropores are small compared with distances over which significant changes in system

variables take place, the two pore systems can be considered separate, one dimensional, homogeneous phases arranged in parallel, with appropriate linking to account for gas transfer from the macropores to the micropore system. Although the dissolved gas concentration in the micropores where they intersect macropores will always be saturated with respect to the pure gas phase, this condition, of course, does not prevail throughout the micropore system. The homogeneous micropore phase is separated from the macropore phase by portions of the micropore system, immediately adjacent to macropores, for which the homogeneous approximation is not valid. In these micropore segments dissolved gas concentration changes very sharply with distance from the macropores; they constitute the "linking pores", joining the macro and micropore phases. This arrangement is shown schematically in Figure 2. The linking pores have the same physical characteristics (diameter, etc.) as the micropores but are not part of the micropore phase.

In this model the dissolved gas concentration is at saturation at the interface between the linking pores and the macropore phase (and in micropores at gas side face of the electrode). At the micropore phase ends of the linking pores it reaches the concentration existing at the position in question in the micropore phase. The lengths of the linking pores are short, of the order of a micropore diameter, since the high degree of cross-connection in the micropores renders the homogeneous approximation valid at greater distances than this from a macropore. At the liquid side face of the electrode, the electrolyte composition in the micropore phase is that of bulk electrolyte.

Electrode Description

The electrode reaction for this model is the general gas reaction

$$G + ne^- \rightarrow \mu H_2O + \nu S_1^{z_1} \qquad (1)$$

where G represents the chemical symbol for some reactant gas and S_1 that for an ionic species of charge z_1 which participates in the reaction; μ and ν are stoichiometric coefficients. A realistic electrode kinetic relationship for this reaction is the Volmer type expression for the transfer current, j_s:

$$j_s = j_o \left\{ \frac{c_g}{c_g^o} \exp\left[\frac{\alpha m F}{RT}(\phi-\phi_e)\right] - \frac{c_1}{c_1^o} \exp\left[\frac{(\alpha-1)mF}{RT}(\phi-\phi_e)\right]\right\}. \qquad (2)$$

This expression is characterized by the exchange current density j_o, and the equilibrium potential ϕ_e at the bulk electrolyte concentration, c_1^o, and gas saturation, c_g^o. It should be noted that the electron transfer in the rate determining step, m, is not necessarily the overall electron transfer, n. All potentials are specified with reference to the isopotential electrode matrix.

The electrode structure is characterized by macro and micropore porosities, Q and q, respectively, and by specific surfaces, A and a. The effective length of the linking pores is designated δ.

In treatment of the electrode model, the following assumptions are invoked:

1. Isopotential electrode matrix.
2. Uniform gas composition in macropores.
3. Absence of hydrodynamic flows.
4. Constant transport parameters.
5. Isothermal operation.

The examination is restricted to cases where only one significant non-reacting ionic species, S_2, is present; this is the case for the binary

electrolytes commonly used with gas electrodes.

The Micropore System

In the micropore phase the transport of dissolved gas by diffusion and of ionic species by diffusion and migration must be considered. Transport of current is by ionic species and is thus taken into account. Using the fundamental flux equations for electrolytes, and incorporating the Nernst-Einstein relation for ionic mobilities ($u_i = D_i/kT$),

$$\frac{\omega}{q} N_g = - D_g \frac{dc_g}{dx} , \tag{3}$$

$$\frac{\omega}{q} N_1 = - D_1 \frac{dc_1}{dx} - z_1 D_1 c_1 \frac{d\Phi}{dx} , \tag{4}$$

$$\frac{\omega}{q} N_2 = - D_2 \frac{dc_2}{dx} - z_2 D_2 c_2 \frac{d\Phi}{dx} , \tag{5}$$

where the N_i are superficial fluxes, the D_i the diffusion coefficients, ω the micropore tortuosity, and $\Phi \equiv F(\phi-\phi_e)/RT$. Noting that electroneutrality must be satisfied, that is $z_1 c_1 + z_2 c_2 = 0$, and that N_2 must be 0 at steady state, we can integrate equation (5) to give

$$c_1 = c_1^o \, e^{-z_2(\Phi-\Phi^o)} , \tag{6}$$

where the reference conditions (c_1^o, Φ^o) are those in the bulk electrolyte. The current density in the micropores, i, is given by $i = z_1 F N_1$.

By conservation of dissolved gas in the micropores

$$\frac{dN_g}{dx} = U_g - U_R ,$$

or

$$\frac{d^2 c_g}{dx^2} + \frac{\omega}{qD_g} (U_g - U_R) = 0 , \tag{7}$$

where U_g and U_R are, respectively, the source term for dissolved gas

entering micropores from the linking pores and the sink term for consumption of gas in reaction at micropore walls (both in gmol/cm^3-s). It should be noted the U_R can be directly related to transfer current density,

$$U_R = \frac{a}{nF}\left(1 - \frac{A\delta}{\omega}\right) j_s \ . \tag{8}$$

Conservation can likewise be applied to ionic species 1, giving, with substitution from equation (6) and the change of variable to $E \equiv e^{z_2(\Phi^o - \Phi)}$;

$$\frac{d^2E}{dx^2} + \frac{\omega z_2 \nu}{qD_1 c_1^o (z_2 - z_1)}\left(U_G - U_g + U_R\right) = 0 \ , \tag{9}$$

where U_G is the sink term, in the macropores, for gas dissolving into linking pores (thus $U_G - U_g$ represent gas reacting, per unit volume of electrode, in linking pores).

Equations (7), (8) and (9), taken together with the boundary conditions

$$\begin{aligned} &\text{at } x = 0: \quad c_g = c_g^o \ , \quad \frac{d\Phi}{dx} = \frac{dE}{dx} = 0 \ ; \\ &\qquad x = \ell: \quad c_g = 0 \ , \quad \Phi = \Phi^o \rightarrow E = 1 \ ; \end{aligned} \tag{10}$$

represent the micropore behavior. However, U_G and U_g are functions of $E(\Phi)$ and c_g and must be determined by consideration of processes occurring in the linking pores.

The Linking Pores

In the linking pores the transport relationships are basically the same as those in the micropores, but here they are applied in a direction, y, normal to local macropore surface rather in the one dimension of the homogeneous phases, x. In the conservation equations the terms U_G and U_g of course do not appear, and, therefore, corresponding to (7) and (9) are the forms

$$\frac{d^2 c_g^*}{dy^2} - \frac{\omega}{qD_g} U_R^* = 0 \tag{11}$$

and
$$\frac{d^2E^*}{dy^2} + \frac{\omega z_2 \nu}{qD_1 c_1^o (z_2 - z_1)} U_R^* = 0 , \qquad (12)$$

where U_R^* is the sink term for use of gas in reaction at the walls of the linking pores. Combining (11) and (12) to eliminate U_R^*, we see that

$$\frac{d^2E^*}{dy^2} = - \frac{D_g z_2 \nu}{D_1 c_1^o (z_2 - z_1)} \frac{d^2 c_g^*}{dy^2} .$$

If c_g^* is normalized to $C^* = c_g^*/c_g^o$, and this expression is integrated once

$$\frac{dE^*}{dy} \propto \left(\frac{D_g c_g^o}{D_1 c_1^o} \right) \left(\frac{\nu z_2}{z_2 - z_1} \right) \frac{dC^*}{dy} .$$

Since $(D_g c_g^o / D_1 c_1^o) << 1$ (perhaps 10^{-5} - 10^{-6}), the changes in E^*, and thus in c_1^*, over the linking pores are relatively much less than the changes in c_g^*. Accordingly E^*, and c_1^*, are considered constant over the length of a linking pore at the values existing at its junction with the micropore phase. Then

$$U_R^* = \frac{a}{nF} j_s = \frac{a}{nF} j_o \left\{ \frac{c_g}{c_g^o} r - b \right\} \qquad (13)$$

where r and b are functions of E, which is now a parameter as far as the linking pores are concerned.

$$r = e^{\alpha m \Phi^o} E^{-\alpha m / z_2} ; \quad b = e^{(\alpha - 1) m \Phi^o} E^{1 - [(\alpha - 1) m / z_2}$$

When this value for U_R^* is substituted in (11) the equation becomes

$$\frac{d^2 c_g^*}{dy^2} - \frac{a \omega j_o}{nFqD_g} \left[\frac{c_g^*}{c_g^o} r - b \right] = 0 , \qquad (14)$$

which is a linear, non-homogeneous, equation with constant coefficients. Its boundary conditions are:

$$\begin{aligned} \text{at} \quad y = 0 : \quad & c_g^* = c_g^o \\ y = \delta : \quad & c_g^* = c_g \end{aligned} \qquad (15)$$

and thus it has the obvious particular integral

$$\frac{c_g^*}{c_g^o} = \frac{b}{r} .$$

Again letting $C^* = c_g^*/c_g^o$, and taking $\theta \equiv a\omega\delta^2 j_o/qnFD_g c_g^o$, we can easily find the complete solution in the form

$$C^* = \frac{b}{r} + K_1 e^{\sqrt{\theta r}(y/\delta)} + K_2 e^{-\sqrt{\theta r}(y/\delta)} . \qquad (16)$$

Actually this solution itself is not of interest since only the terms U_G and U_g are required. They depend on the derivatives at $y = 0$ and $y = \delta$, since they are proportional to dissolved gas fluxes at these points.

$$U_G = \frac{AqD_g c_g^o}{\omega} \left(-\frac{dC^*}{dy}\right)_{y=0} \qquad (17)$$

$$U_g = \frac{AqD_g c_g^o}{\omega} \left(-\frac{dC^*}{dy}\right)_{y=\delta} . \qquad (18)$$

Therefore the derivatives of C^* with respect to y are found from (16) with appropriate values of the constants K_1 and K_2 to satisfy boundary conditions (15). These are

$$\left(\frac{dC^*}{dy}\right)_{y=0} = -\sqrt{\theta r}\,\frac{1}{\delta}\left\{\frac{1}{\sinh\sqrt{\theta r}}\left[\left(1-\frac{b}{r}\right)e^{-\sqrt{\theta r}} - \left(C-\frac{b}{r}\right)\right] + \left(1-\frac{b}{r}\right)\right\} \qquad (19)$$

$$\left(\frac{dC^*}{dy}\right)_{y=\delta} = -\sqrt{\theta r}\,\frac{1}{\delta}\,\frac{\cosh\sqrt{\theta r}}{\sinh\sqrt{\theta r}}\left[\left(1-\frac{b}{r}\right)e^{-\sqrt{\theta r}} - \left(C-\frac{b}{r}\right)\right] + \left(1-\frac{b}{r}\right)e^{-\sqrt{\theta r}}\Bigg\} . \qquad (20)$$

Together with (17) and (18) these expressions yield the necessary source terms to complete the model description.

Mathematical Representation of Electrode Model

The mathematical statement of the model is put in more compact form by change to the dimensionless variables,

$$X = \frac{x}{\ell} \; ; \quad C = \frac{c_g}{c_g^o} \; ; \quad E = e^{(\phi^o - \phi) z_2 F/RT} \; ,$$

the latter two of which have previously been introduced for convenience. The source/sink terms are also put in non-dimensional form:

$$W_G = \frac{\omega\delta^2}{qD_g c_g^o} U_g \; ; \quad W_g = \frac{\omega\delta^2}{qD_g c_g^o} U_g \; ; \quad W_R = \frac{\omega\delta^2}{qD_g c_g^o} \; .$$

These changes of variable give rise to the dimensionless parameters of the system:

$$L = \frac{\ell}{\delta} \qquad \lambda = A\delta$$

$$\theta = \frac{a\omega\delta^2 j_o}{qnFD_g c_g^o} \qquad \eta = \left(\frac{z_2^{\nu}}{z_2 - z_1}\right)\left(\frac{D_g c_g^o}{D_1 c_1^o}\right) \; .$$

In this notation, the electrode model as embodied in equations (2), (7), (8), (9), (17), (18), (19), and (20) becomes:

$$\frac{d^2C}{dX^2} + L^2(W_g - W_R) = 0 \tag{21}$$

$$\frac{d^2E}{dX^2} + \eta L^2(W_G - W_g + W_R) = 0 \tag{22}$$

$$W_G = \lambda f E^{-\beta}\left\{\left[\frac{1}{\sinh fE^{-\beta}}\right]\left[(1-gE^{\gamma})e^{-fE^{-\beta}} - (C-gE^{\gamma})\right] + (1-gE^{\gamma})\right\}$$

$$W_g = \lambda f E^{-\beta}\left\{\left[\frac{1}{\tanh fE^{-\beta}}\right]\left[(1-gE^{\gamma})e^{-fE^{-\beta}} - (C-gE^{\gamma})\right] + (1-gE^{\gamma})e^{-fE^{-\beta}}\right\} \tag{23}$$

$$W_R = (1-\lambda) f^2 E^{-2\beta}(C-gE^{\gamma})$$

where the expressions: $f \equiv \theta^{1/2}\, e^{\alpha m\Phi^o/2}$; $g \equiv e^{-m\Phi^o}$; $\beta \equiv \alpha m/2z_2$; and $\gamma \equiv 1 + m/z_2$ have been introduced for compactness. Equations (21) and (22) have the boundary conditions:

$$\text{at } X = 0: \quad C = 1; \quad \frac{dE}{dX} = 0$$
$$X = 1: \quad C = 0; \quad E = 1. \tag{24}$$

This pair of second order ordinary differential equations completely describes the model for the double porosity scale electrode. Analysis and predictions for electrode behavior are based upon solutions of this equation system. The dimensionless current density at any position, X, in the micropore phase of this system is

$$I = L\int_0^X (W_G - W_g + W_R)\, dX$$

where $I = (\theta/a\delta)(i/j_o)$.

Analysis of the Electrode Model

The equation system (21) and (22) with source terms (23) and boundary conditions (24) is not amenable to analytic solution because of the non-linear nature of the source terms. Numerical techniques are required for analysis of the mathematical model. The numerical method employed consists essentially in representing the derivatives in (21) and (22) by their second order (central) finite difference forms, thus obtaining a set of simultaneous, non-linear, algebraic equations, two for each finite difference point employed. These equations are solved by a simultaneous first order (point-slope) iteration process, starting with an approximate solution for the equations.

The solution used as a starting point for this iteration is an approximate analytic solution derived for the situation where reaction in the linking pores is disregarded. As the total reaction surface in the linking pores is small compared with that in the micropore phase, it should be expected that this approximation will be sufficiently

accurate to provide convergence for the first order iteration scheme. This has proved to be the case.

The computations are implemented with an IBM 7094 computer through a FORTRAN IV program. The iterative procedure converges in very few (less than five) iterations, although final solutions usually deviate considerably from the approximations used as initial estimates.

APPLICATION TO THE OXYGEN CATHODE

The model described in the previous section has been applied to an oxygen cathode operating in 6.9 N KOH (at 25°C) in order to examine the nature of its predictions and the influence of structural parameters. As a basis for these calculations, electrode kinetic parameters characteristic of oxygen reduction on silver were used[10]. These are listed, together with the necessary transport and concentration values, in the table below.

Parameters for Oxygen Cathode in 6.9 N KOH at 25°C

Electrode Reaction: $O_2 + 2H_2O + 4e^- \rightarrow 4OH^-$

Electrons transferred in rate determining step (m)	1
Transfer coefficient (α)	1/2
Exchange current density (j_o)	$2 \times 10^{-6} A/cm^2$
Diffusion coefficient of OH^- ion (D_l)	$2 \times 10^{-5} cm^2/s$
Diffusion coefficient of dissolved O_2 (D_g)	$0.6 \times 10^{-5} cm^2/s$
Oxygen solubility for 1 atm pressure (c_g^o)	$7 \times 10^{-5} gmol/L$

The electrode structure selected for this example was 0.1 cm thick and had a macroporosity of 30% with 2μ diameter pores and a microporosity of 30% with 0.1μ diameter pores. Corresponding macro and micropore specific surface areas are 600 and $1.2 \times 10^5 cm^{-1}$, respectively. A tortuosity factor of 2 was used. The linking pore length, δ, was assumed

to be one micropore diameter (0.1μ); however, because of the uncertainty in the proper value to use for this dimension, the effects of variations in assumed linking pore length were investigated.

Electrode Overpotential Behavior

The calculated current density/electrode overpotential behavior for this electrode is presented as the curve A in Figure 3. The behavior predicted using linking pore lengths of half and twice the micropore diameter is also shown, by curves B and C. It is apparent that the calculated current densities are sensitive to assumed linking-pore length at high overpotentials but that the nature of the current density/overpotential relationship is unaffected by this choice.

The overpotential curve is not even approximately linear in a log (current density) vs overpotential plot; it cannot be characterized by a "Tafel slope" over any significant portion of its range. As a matter of fact, the behavior is quite nearly linear, as shown in Figure 4. This pattern is the result of the reduced dissolved gas concentrations in the micropore system at higher electrode currents in part offsetting the almost exponential reaction rate increases with increasing overpotential.

The overpotential behavior of this model is compared in Figure 3 with that of a "film model"[2] operating with a 0.1μ film in the macropores, curve D. This latter model would represent the electrode if it possessed only a single scale of porosity, that of the macropore system. As should be expected the double porosity scale model predicts much higher electrode currents throughout the operating range than does the film model. It should also be noted that the film model gives rise to a log (current density) vs overpotential relationship which is linear over an appreciable part of the overpotential range, in contrast to the behavior of the present model,

which was discussed above.

Changes in micropore porosity have no effect on the overpotential behavior other than to scale the current density in proportion to this porosity. Changes in the macropore porosity have little effect until this porosity becomes quite small (<0.1). For very low macroporosities the activity of the electrode becomes quite small, and the shape of the overpotential curve approaches linearity on a log (current density) vs overpotential plot. This is illustrated, for $Q = 10^{-4}$, by curve E in Figure 3.

Reaction Distribution

The distribution of the cathodic reaction in depth in the electrode is nearly uniform for any realistic electrode operation. This is depicted in Figure 5 for 100mV overpotential. The reaction rate is high in the portion of the electrode immediately adjacent to the gas side face because of ready access to dissolved gas at this face. At greater depths in the electrode it quickly drops to a rate near the average and then increases gradually with depth as a result of the corresponding decrease in ionic current path lengths. Very near the liquid side face of the electrode the rate suddenly decreases drastically as dissolved gas concentrations become vanishingly low because of losses to the bulk electrolyte.

The reaction rate in the linking pores is only a small fraction of the total rate but exhibits a similar distribution as also shown in Figure 5. The linking pores will contribute a significant part of the overall current only if they are assumed to be very long (many micropores diameters) or if very high overpotentials are used (>300mV).

CONCLUSIONS

This study has established a mathematical model for porous gas electrodes with two superimposed scales of porosity, a model which predicts

the high current densities often achieved in modern gas electrodes, most of which have such a structure. The performance of these highly active electrodes (e.g.[6]) cannot be explained on the basis of film or surface diffusion models developed for single pore scale structures.

The current density/overpotential relationships calculated with this model are approximately linear over a wide overpotential range, in contrast with the exponential behavior predicted by film models using realistic kinetic expressions. This linear polarization characteristic holds only so long as an appreciable macroporosity is present; as the extent of the gas filled pore system becomes small the electrode effectiveness decreases to a very low level, and the linear current density:overpotential curve changes to a nearly exponential behavior. The nature of performance predictions of this model are insensitive to the linking pore length used in the calculations. However, the quantitative predictions at higher overpotentials are significantly affected by this value, the choice of which cannot easily be made a priori. Thus at least this parameter in the model must be adjusted on the basis of measurements conducted with the electrode in question.

The reaction distribution in the double porosity scale electrode is very nearly uniform over the thickness of the electrode. This characteristic is primarily responsible for the high activity of this type of electrode and represents a very efficient use of electrode (and catalytic) material and space.

The model developed here presents the possibility for a comprehensive investigation of the effects of porosity distribution in gas electrodes of multiple porosity scale. Such work, which is presently in progress, may lead to design criteria for structure of more efficient electrodes.

In addition, similar linked phase models can be applied to other systems of multiple porosity scale, such as those encountered in catalytic reactions in packed beds.

ACKNOWLEDGEMENT

This work was performed under the auspices of the United States Atomic Energy Commission.

NOMENCLATURE

A,a = macro/micropore specific surface areas (cm^{-1})

C = c_g/c_g^o

c_i = concentration of species i ($gmol/cm^3$)

D_i = diffusion coefficient for species i (cm^2/s)

E = $\exp [F(\phi^o-\phi)/RT]$

F = Faraday constant (coul/equiv)

I = $\theta i/a\delta j_o$

i = superficial current density (A/cm^2)

j_o = exchange current density (A/cm^2)

j_s = transfer current density (A/cm^2)

k = Boltzman constant

L = ℓ/δ

ℓ = electrode thickness (cm)

m = number of electrons transferred in rate determining step

N_i = superficial flux of species i ($gmol/cm^2$-s)

n = stoichiometric number of electrons transferred

Q,q = macro/microporosity

R = gas constant (cal/gmol-°K)

T = absolute temperature (°K)

U_G,U_g,U_R = dimensional source terms ($gmol/cm^3$-s)

u_i = mobility of species i (cm/sec-dyne)

W_G,W_g,W_R = dimensionless source terms

X = x/ℓ

x = depth coordinate (cm)

y = link pore length coordinate (cm)

z_i = charge number of species i

α = transfer coefficient

δ = linking pore length (cm)

$\eta = z_2 \nu D_g c_g^o / (z_2 - z_1) D_1 c_1^o$

$\theta = a\omega\delta^2 j_o / qnFD_g c_g^o$

$\lambda = A\delta$

μ, ν = stoichiometric coefficients

$\Phi = F(\phi - \phi_e)/RT$

ϕ = potential with respect to electrode matrix (V)

ω = tortuosity factor

Subscripts:

g = dissolved gas

1 = reacting ion

2 = counter ion

e = equilibrium conditions

Superscripts:

o = in bulk electrolyte

* = in linking pores

LITERATURE CITED

1. Burshtein, R. C., Markin, V. S., Pshenichnikov, A. G., Chismadgev, V. A., and Chirkov, Y. G., Electrochimica Acta 9, 773 (1964).

2. Grens, E. A., Turner, R. M., and Katan, T., Advanced Energy Conversion 4, 109 (1964).

3. Iczkowski, J. Electrochem. Soc. 111, 1078 (1964).

4. Justi, E., Pilkuhn, M., Scheibe, W., and Winsel, A., "High-Drain Hydrogen-Diffusion-Electrodes Operating at Ambient Temperature and Low Pressure", Verl. d. Akad. d. Wissensch. u.d. Lit., Wiesbaden (1959).

5. Katan, T., Szpak, S., and Grens, E. A., "An Experimental Study of the Operation of a Porous Oxygen Cathode", in press for J. Electrochem. Soc.

6. Niedrach, L. W., and Alford, H. R., J. Electrochem. Soc. 112, 117 (1965).

7. Paxton, R. R., Demendi, J. F., Young, G. J., and Rozelle, R. B., J. Electrochem. Soc. 110, 932 (1963).

8. Wagner, C., Max-Planck-Institut für physikalische Chemie, Göttingen, Germany; unpublished, 1957.

9. Will, F. G., J. Electrochem. Soc. 110, 152 (1963).

10. Winsel, A. W., Advanced Energy Conversion 3, 427 (1963).

FIGURE TITLES

Figure 1 Representation of gas electrode with double scale of porosity (greatly enlarged-not to scale).

Figure 2 Model for gas electrode with double scale of porosity.

Figure 3 Calculated current density/overpotential behavior for oxygen cathode (log current scale).

Figure 4 Calculated current density/overpotential behavior for oxygen cathode (linear current scale).

Figure 5 Calculated reaction distribution for oxygen cathode - 100mV Overpotential.

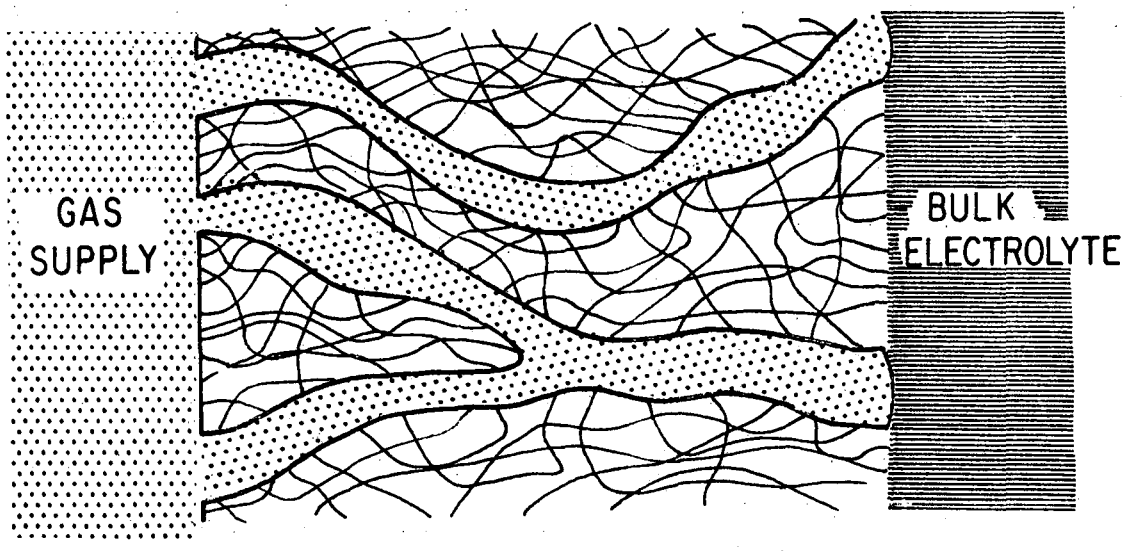

Fig. 1

MUB-8673

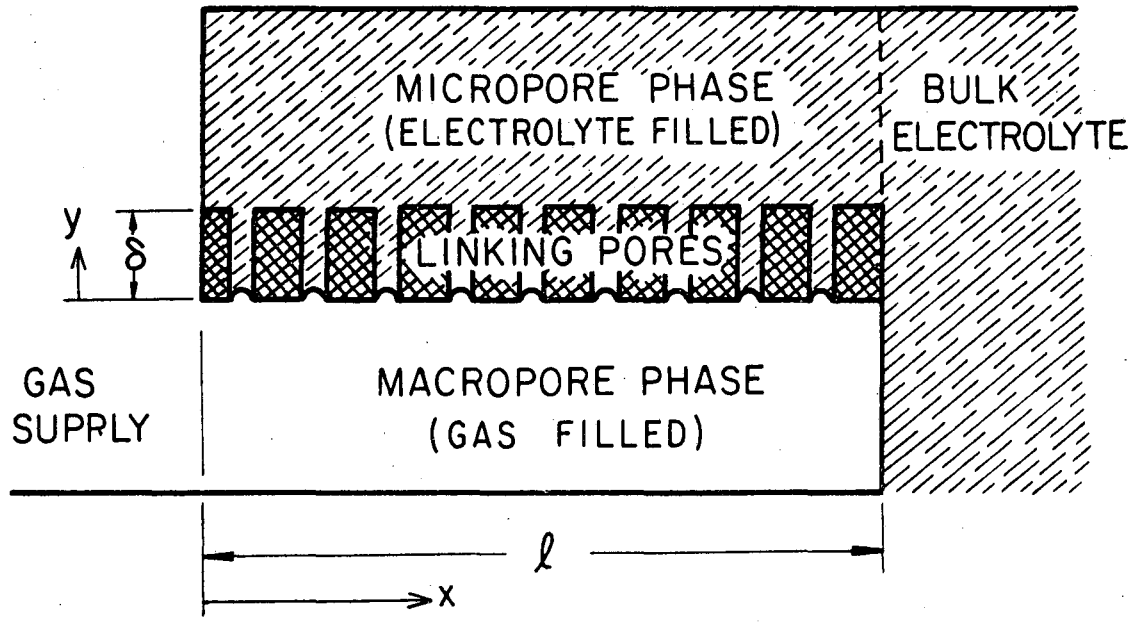

Fig. 2

MUB-8671

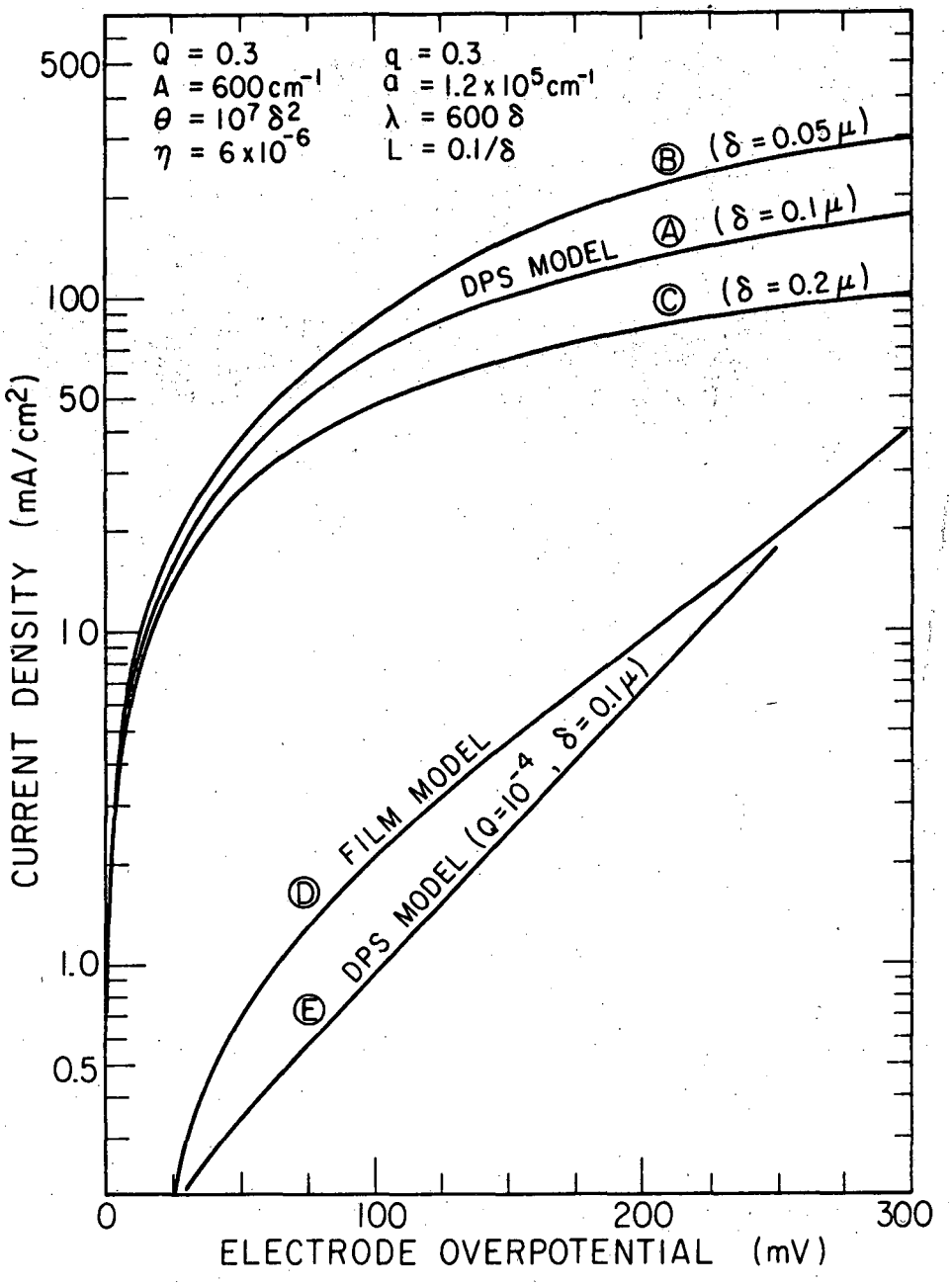

Fig. 3

MUB-8669

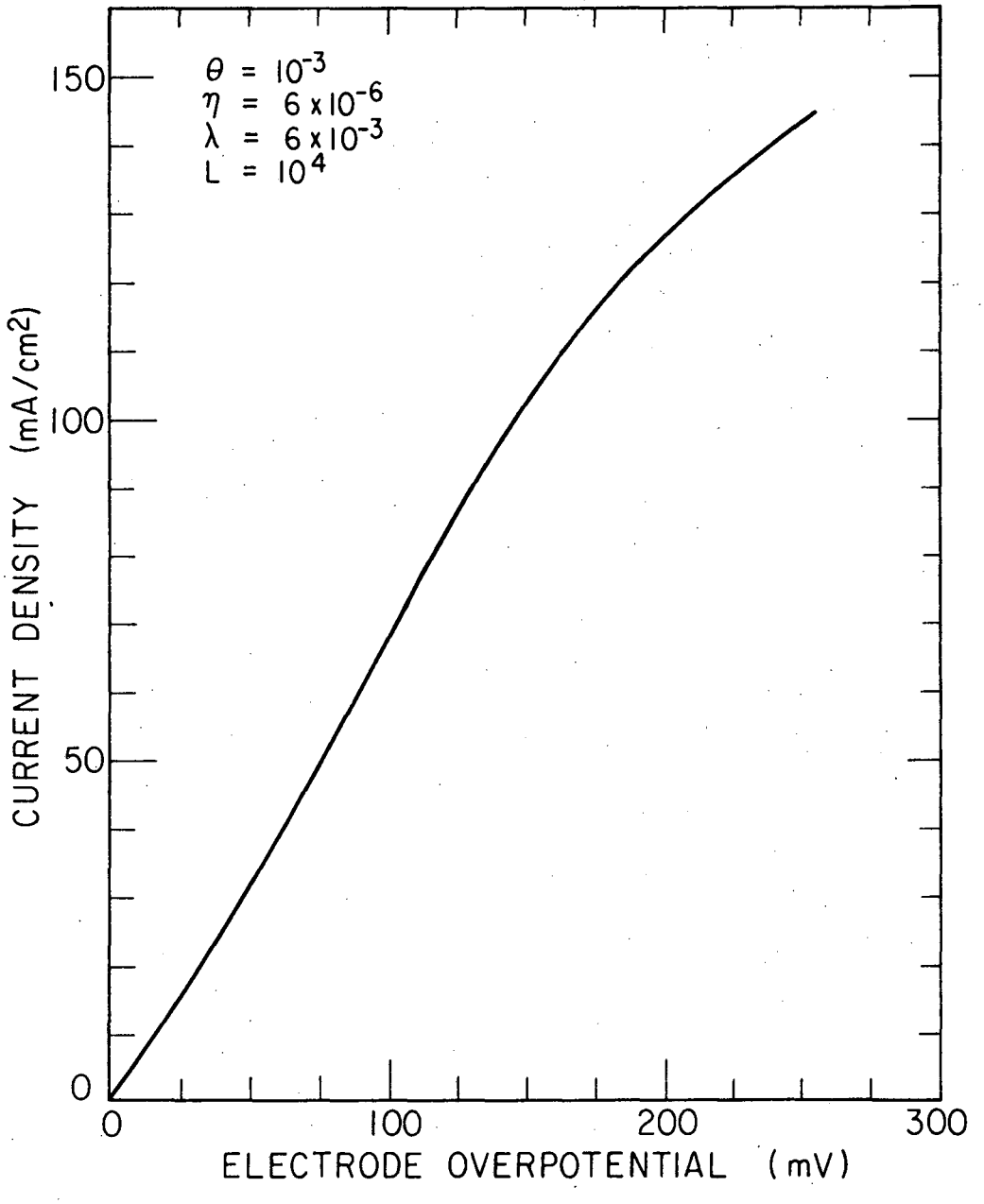

Fig. 4

MUB-8670

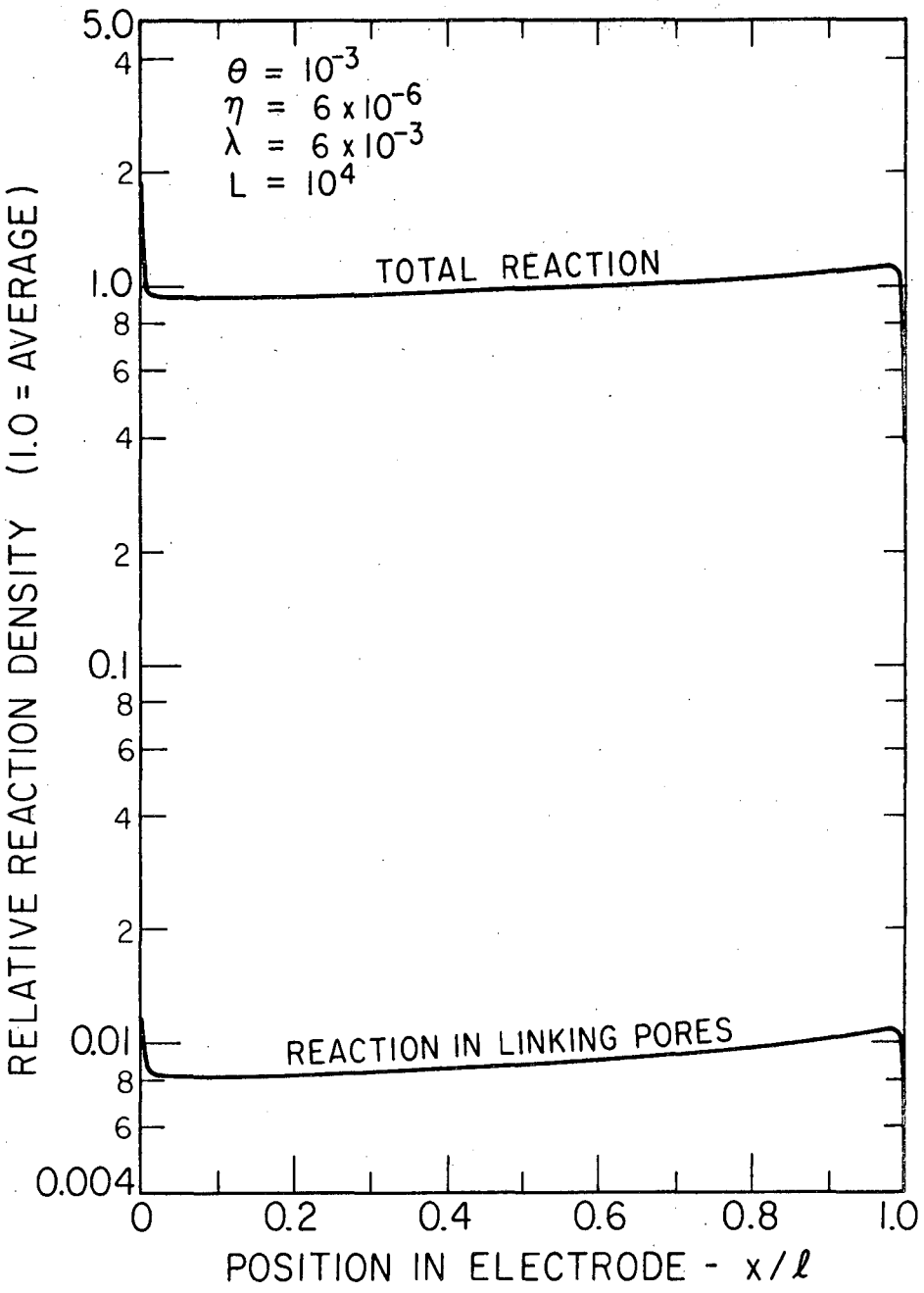

Fig. 5 MUB-8672